

NASA TECHNICAL NOTE



NASA TN D-5318

NASA TN D-5318



EFFECT OF FLUID TEMPERATURE ON
THE CAVITATION PERFORMANCE OF A
HIGH HUB-TIP RATIO AXIAL FLOW PUMP
IN WATER TO 250° F (394 K)

*by Walter S. Cunnan, George Kovich, and Dean C. Reemsnyder
Lewis Research Center
Cleveland, Ohio*



EFFECT OF FLUID TEMPERATURE ON THE CAVITATION
PERFORMANCE OF A HIGH HUB-TIP RATIO AXIAL
FLOW PUMP IN WATER TO 250⁰ F (394 K)

By Walter S. Cunnan, George Kovich, and Dean C. Reemsnyder

Lewis Research Center
Cleveland, Ohio

NATIONAL AERONAUTICS AND SPACE ADMINISTRATION

For sale by the Clearinghouse for Federal Scientific and Technical Information
Springfield, Virginia 22151 - CFSTI price \$3.00

ABSTRACT

An axial flow pump was tested in deaerated water at temperatures to 250° F (394 K). Noncavitation performance is independent of fluid temperature in this range. A reduction in the required net positive suction head of 2.0 to 6.0 feet (0.6 to 1.8 m) was measured in 250° F (394 K) water under that in 80° F (300 K) water at similar operating conditions. This improvement in cavitation performance increases with increasing flow coefficient and decreasing head-rise coefficient ratios. Cavitation formations in the rotor were visually observed and photographed in 80° F (300 K) water. Slight suction surface cavitation damage occurred near the tip leading edges during the 162 hours of operation.

EFFECT OF FLUID TEMPERATURE ON THE CAVITATION PERFORMANCE OF A HIGH HUB-TIP RATIO AXIAL FLOW PUMP IN WATER TO 250° F (394 K)

by Walter S. Cunnan, George Kovich, and Dean C. Reemsnyder

Lewis Research Center

SUMMARY

An axial flow pump was tested in deaerated water at temperatures to 250° F (394 K). The 5-inch (12.70-cm) research rotor had nine double circular arc blades, a blade tip diffusion factor of 0.40, a hub-tip radius ratio of 0.77, and a blade tip solidity of 1.0.

Noncavitation and cavitation performance of the rotor and pump was obtained in room temperature deaerated water at rotative speeds of 5000, 7200, and 8500 rpm. Additional performance was obtained at 7200 rpm for fluid inlet temperatures of 175° and 250° F (353 and 394 K). The cavitation formations in the rotor were observed and photographed in 80° F (300 K) water through a transparent plastic window over the test rotor.

Noncavitation performance of the pump and rotor is independent of fluid temperature to 250° F (394 K). An inflection of the head-flow characteristic curve occurs near the design flow coefficient. Overall pump head rise is less than the rotor head rise due to losses in the pump inlet, outlet vaneless diffuser, and volute collector.

Cavitation performance of the pump and rotor are independent of fluid temperature to 175° F (353 K). Initial head-rise dropoff occurs at suction specific speeds of 5500 to 6000 because of tip vortex cavitation. A reduction in the required net positive suction head of 2.0 to 6.0 feet (0.6 to 1.8 m) was measured at 250° F (394 K) under that at 80° F (300 K). This improvement in cavitation performance is attributed to the thermodynamic effects of cavitation and it increases with increasing flow coefficient and decreasing head-rise coefficient ratio. At a head-rise coefficient ratio of 0.90 and at the design flow coefficient, the measured reduction in required net positive suction head was 2.9 feet (0.9 m) in 250° F (394 K) water.

Visual and photographic observations indicate that tip vortex cavitation increased in volume and moved rearward with decreasing net positive suction heads. Head-rise dropoff occurred when this tip vortex cavitation covered about the outer third of the blade passage. Slight suction surface and tip vortex cavitation occurred near the blade tip leading edges, where the rotor sustained slight cavitation damage. Total operating time was 162 hours, of which 72 hours were in cavitation.

INTRODUCTION

Cavitation is a major concern in many pumping applications because it can result in reduced pump performance and/or impeller blade damage. Cavitation performance can be dependent upon the fluid and its operating temperature. This dependency can result in a performance change and a lower required net positive suction head to the pump and is referred to as a thermodynamic effect of cavitation. The magnitude of the decrease is dependent upon the physical and thermodynamic properties of the fluid, as well as the vapor distribution, pump design, rotative speed, and flow coefficient.

In reference 1 the required net positive suction head for a cavitating inducer was considerably less in 37⁰ R (20.5 K) hydrogen than that for a similar inducer in room temperature water. Reference 2 presents an empirical method of determining the cavitation performance of small low suction specific speed centrifugal pumps. The method is based on cavitation tests using deaerated water to 300⁰ F (421 K), several hydrocarbons, Freon, and other fluids.

During the cavitation process, vapor forms in a flowing liquid when the local static pressure falls below the vapor pressure of the local fluid. Heat required to form the vapor cavity must come from the surrounding liquid. During the vaporization process, the liquid in a thin layer adjacent to the cavity is cooled. The extent of this cooling depends on the properties of the liquid and the flow conditions. For a pump, this can result in lower required net positive suction heads at increased liquid temperatures. In the Venturi studies of reference 3, for similar cavities the change in the depression of the cavity pressure below fluid inlet vapor pressure was equal to the change in the inlet pressure requirements. Thus the decrease in required inlet pressure is a measure of the thermodynamic effect of cavitation.

The thermodynamic effect of cavitation for a pump in any fluid is defined herein as the difference between the required net positive suction head for a given liquid and temperature and that obtained in room temperature water under similar flow conditions. This infers constant rotative speed, constant flow coefficient, and the same head-rise coefficient ratio. It is assumed that the same vapor volume exists at the same head-rise coefficient ratio (refs. 3, 4, and 5). This provides the same vapor blockage in the flow passage and maintains a constant ratio of fluid to blade velocity. This assumption can be affected by the type of cavitation in a pump.

The rotor used in this investigation is identical, except for direction of rotation, to a rotor previously tested in liquid sodium to temperatures of 1500⁰ F (1089 K), as reported in reference 6. This evaluation of pump performance and blade cavitation damage in liquid sodium was in support of the condensate pump development for alkali metal

Rankine cycle space electric power systems.

The objective of this investigation is to determine the effect of fluid temperature on the cavitation performance of an axial flow pump in water over a range of flow coefficients. Cavitating performance was evaluated in room temperature water at rotor speeds of 5000, 7200, and 8500 rpm. Evaluation of cavitating performance at the rotor speed of 7200 rpm was extended to water temperatures of 175^o and 250^o F (353 and 394 K). The rotor was tested in deaerated water over a range of flow coefficients from 0.09 to 0.21 and net positive suction heads from 20 to 210 feet (6.1 to 64.0 m). The cavitating formations in the rotor were observed and photographed in room temperature water.

ROTOR DESIGN

The hydrodynamic design of the axial flow rotor is identical to that reported in reference 6 except for direction of rotation. A pretest photograph of the 316 stainless-steel integral-bladed rotor is shown in figure 1. A tabulation of the rotor dimensions and other pertinent rotor design parameters is given in table I.

This rotor design is presented in detail in reference 6; only a brief resumé is presented herein. The design procedure utilized a blade element concept with design calculations made across blade elements at a selected number of radial positions. These elements were arranged with their centers of gravity on a radial line to form the blade.

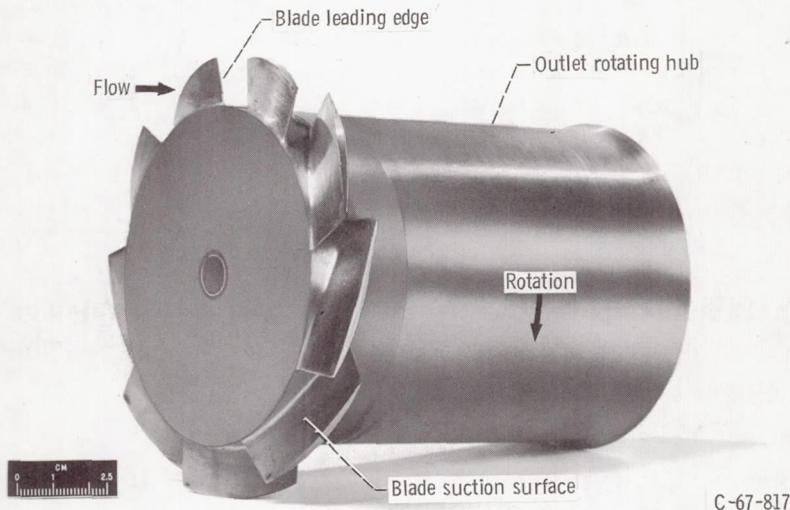


Figure 1. - Axial flow rotor.

TABLE I. - BLADE DESIGN PARAMETERS
OF AXIAL FLOW ROTOR

Rotor design conditions	
Flow coefficient	0.147
Head-rise coefficient	0.21
Rotor geometry	
Tip diameter, in. (mm)	4.956 (126.0)
Hub-tip radius ratio	0.77
Number of blades	9
Blade tip radial clearance, in. (mm)	0.033 (0.84)
Leading and trailing edge radii, in. (mm)	0.010 (0.254)
Tip geometry (double circular-arc sections)	
Solidity, σ_t	1.00
Diffusion factor, D_t	0.40
Chord length, c, in. (mm)	1.743 (44.3)
Ratio of maximum thickness to chord	0.06
Stagger angle with respect to axis, deg	76.5
Camber angle, deg	4.0
Incidence angle, deg	2.8
Deviation angle, deg	3.8
Inlet blade angle, deg	78.5
Hub geometry (double circular-arc sections)	
Solidity, σ_h	1.30
Diffusion factor, D_h	0.60
Chord length, c, in. (mm)	1.743 (44.3)
Ratio of maximum thickness to chord	0.08
Stagger angle with respect to axis, deg	70.5
Camber angle, deg	19.4
Incidence angle, deg	-1.7
Deviation angle, deg	8.9
Inlet blade angle, deg	81.0

The velocity diagrams were constructed utilizing the following design considerations and assumptions:

- (1) Constant inlet axial fluid velocity at all blade radii
- (2) Constant energy addition at all blade radii
- (3) Simplified radial equilibrium
- (4) Constant blade element efficiency

The basic design procedure follows that presented in reference 7 and utilizes design information from reference 8.

APPARATUS AND PROCEDURE

Test Facility

The experimental data included in this report were obtained by operating the research pump in a closed-loop pump test facility (fig. 2). The flow path is outlined in the schematic diagram of the pump loop (fig. 3). In the main pump loop, the flow passes successively through the research pump, the Venturi flowmeter, test water cooler, and

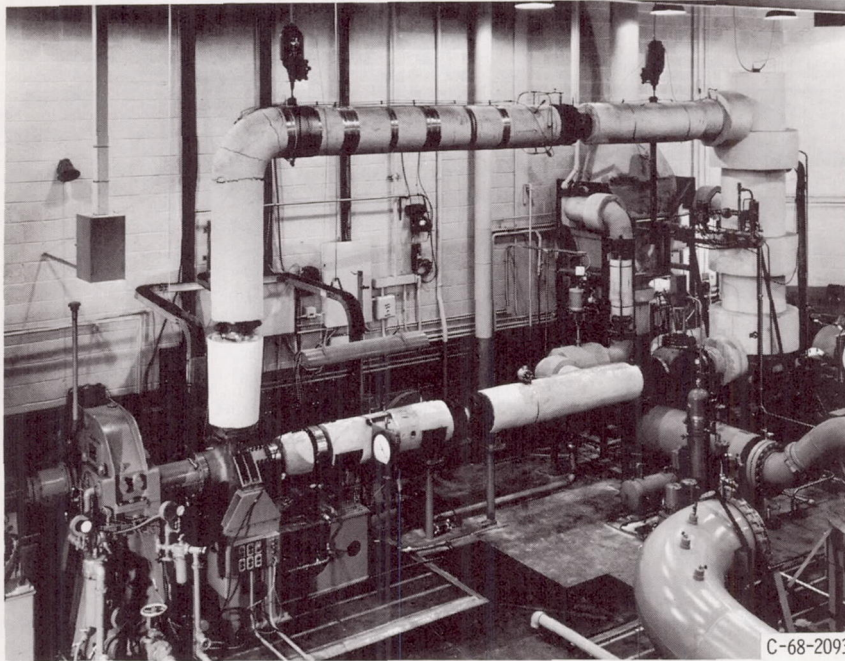


Figure 2. - Photograph of Lewis high-temperature water tunnel.

the noncavitating flow control valve. The water heater is located in a bypass loop across the flow control valve. Water temperature is controlled with a counter-flow heat exchanger. A bank of 16 pressure accumulators controls the research pump inlet pressure. The accumulators also provide volume for thermal expansion of the water in the research loop at elevated temperatures. A 3000-horsepower variable frequency electric motor drives the research pump through a speed increasing gearbox. All facility control systems are automated.

The test water is demineralized to a minimum resistance value of 1 000 000 ohm-centimeters and is supplied to the test loop through a 5-micron filter. The test water is degasified in a bypass system as shown in figure 3. The water flows into a tank at a high vacuum, then is refiltered as it is pumped back into the loop. The gas content of the water can be reduced to 1 part per million by weight. During these tests, the water was degasified to less than 3 parts per million.

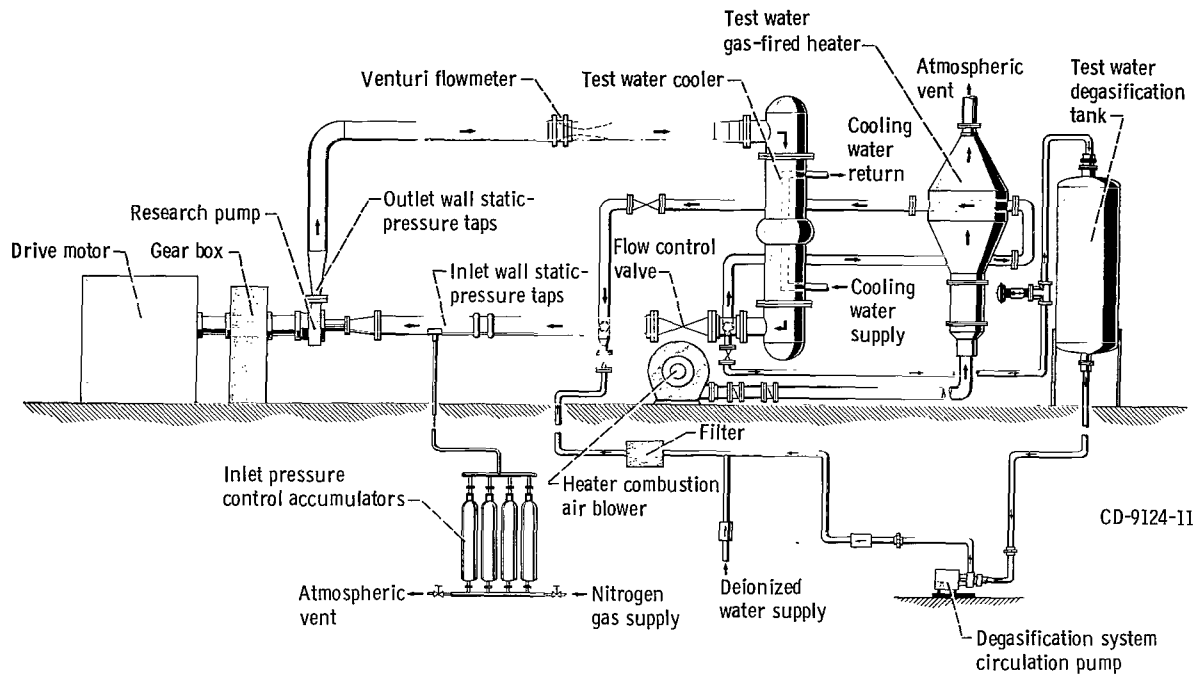


Figure 3. - Schematic of Lewis high-temperature water tunnel.

Research Pump

A cutaway view of the research pump installation is shown in figure 4. The pump consists of a stationary inlet centerbody, the axial flow rotor, an outlet rotating hub, a stationary outlet vaneless diffuser, and a volute collector. The cantilevered rotor is located downstream of the stationary inlet centerbody, which is supported in the water stream by three low-drag struts. A carbon face seal behind the outlet rotating hub prevents internal flow leakage. Survey pressure probes are located at stations 1 and 2 ahead of and behind the rotor in the annulus. A transparent plastic window is used for photographs of cavitating flow in the rotor blade passage.

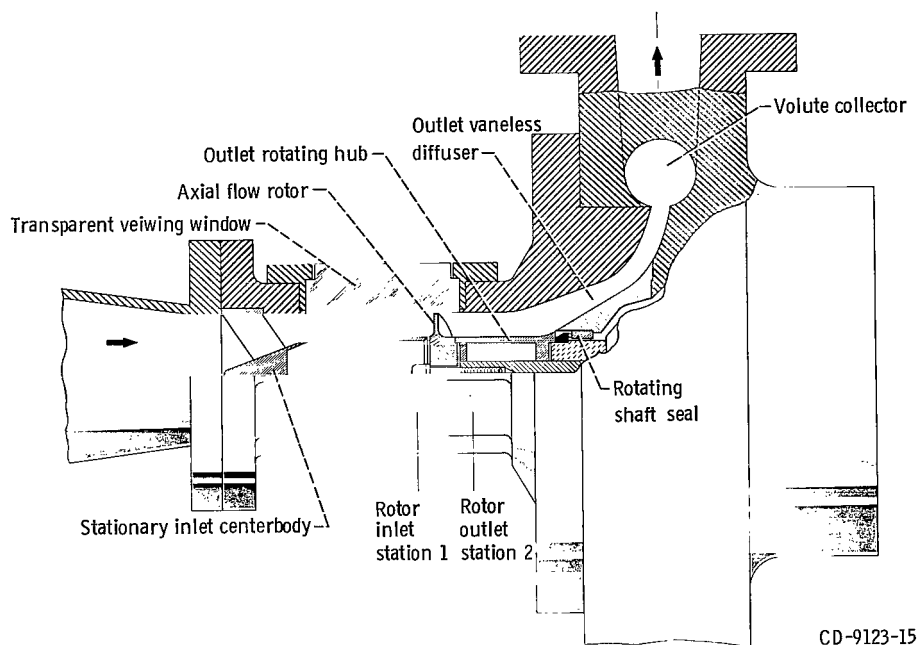


Figure 4. - Cutaway drawing of research pump.

Instrumentation

All pressures are measured with linear strain gage pressure transducers. Water temperatures at the research pump inlet and at the Venturi meter inlet are measured with sealed-type copper-constantan thermocouples. Rotative speed is determined with a frequency counter in conjunction with a magnetic pickup. Flow rate is measured with an ASME short-radius nozzle Venturi meter. Pipe wall static-pressure taps were located upstream of the research pump inlet and at the outlet of the volute collector.

Radial surveys were made with static- and total-pressure probes mounted in probe actuators 1 inch (2.54 cm) upstream and 1 inch (2.54 cm) downstream of the rotor blade row (stations 1 and 2, fig. 4). Each probe included a null-balancing stream direction-sensitive element, which automatically aligned the probe to the direction of flow. A calibrated precision linear potentiometer measured the resulting angular position of each probe. The pressure calibration factor of each static wedge probe was determined in an air tunnel and applied to the measured static pressures in the water tunnel.

All instrumentation outputs were recorded on paper tape through a digitizing potentiometer. The estimated accuracy of the instrumentation is tabulated in table II.

Photographs of the cavitating flow within the rotor blade row were obtained through a transparent plastic window mounted in the research pump test section. A 70-millimeter

TABLE II. - INSTRUMENTATION

Parameter	Experimental range	Error
Flow rate, gal/min (m^3/sec)	200 to 800 (0.0126 to 0.0504)	± 1 percent
Rotative speed, rpm	5000 to 8500	± 0.5 percent
Flow angles, deg	-20 to 120	± 0.5
Heads (ΔH or absolute head), ft (m)	0 to 200 (0 to 61)	± 1 (± 0.31)
Water temperature, $^{\circ}\text{F}$ (K)	80 to 250 (300 to 394)	± 0.5 (± 0.3)

still camera was synchronized with a stroboscopic capacitor discharge flash lamp. A magnetic pickup referenced to a specific position on the rotor shaft circumference provided one pulse per rotor revolution to trigger the camera and flash lamp simultaneously.

Procedure

Pump noncavitating performance was obtained by varying the flow while maintaining a constant rotor speed and a high value of net positive suction head. High flow operation was limited by the open position of the flow control valve. Low flow operation was terminated when measured rotor outlet flow angles were equal to or exceeded 90° . Calculations of performance based on survey data obtained in this region of operation were unreliable because of flow reversals.

Pump cavitation performance was obtained by holding a constant rotor speed and flow, while reducing the pump inlet pressure from the noncavitating performance value. The inlet pressure was varied from a high level judged to be noncavitating to low inlet pressure levels which resulted in the head rise decreasing to 0.7 or less of the noncavitating head rise. Cavitation performance was obtained near the design flow coefficient of 0.147 and the off-design flow coefficients of 0.118 and 0.173 for each pump speed and/or temperature. To determine the effect of pump speed on noncavitation and cavitation performance, tests were conducted in 80°F (300 K) water at rotor speeds of 5000, 7200, and 8500 rpm. The effects of fluid temperature on the noncavitation and cavitation performance were obtained at a rotative speed of 7200 rpm at temperatures of 80° , 175° , and 250°F (300, 353, and 394 K).

All pump and rotor parameters are defined in the symbol list (appendix A). The equations used to calculate the rotor and pump performance are presented in appendix B.

Assumptions used in the rotor performance calculations include no inlet whirl and axisymmetric flow conditions in the annulus before and after the rotor. Data were obtained with the total- and static-pressure probes at preprogrammed radial positions located 10, 30, 50, 70, and 90 percent of passage height from the tip. These data were mass averaged over the annulus area to obtain the overall rotor performance. A detailed discussion of the rotor computations is presented in reference 7.

Overall pump performance is measured from the pump inlet to the outlet of the volute collector. Total pressures were obtained by adding the corresponding dynamic pressures to the wall static pressures measured at locations indicated in figure 4. Experimental data were reduced and corrected to account for thermal expansion of pump

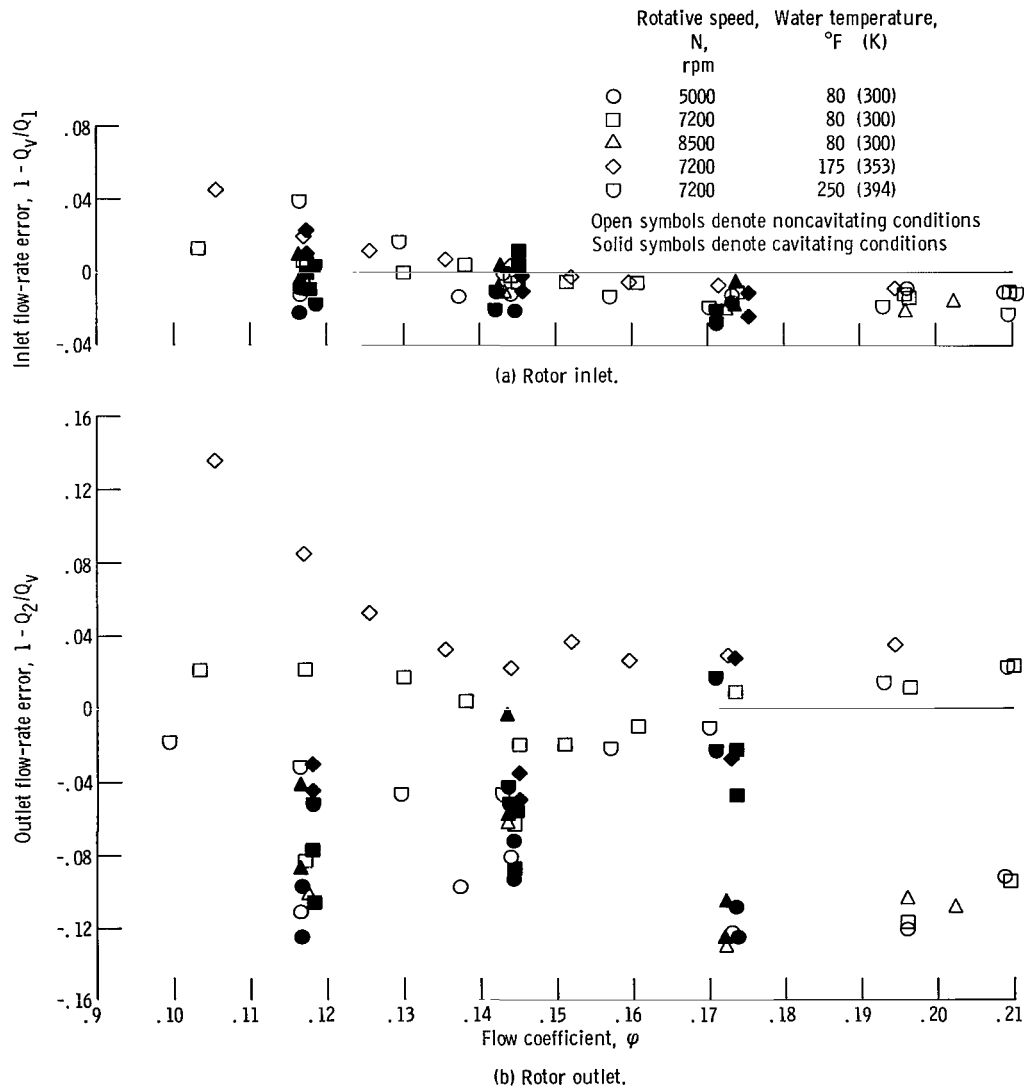


Figure 5. - Comparison of integrated flow with flow measured by Venturi flowmeter.

parts and the Venturi flowmeter, and the change in water properties (density, vapor pressure, and viscosity) as a function of temperature.

Some measure of the reliability of the data is obtained by comparison of the integrated volume flows at the inlet and outlet of the rotor with the volume flow as measured by the Venturi flowmeter. At the rotor inlet most of the integrated flows agree with the measured Venturi flows within ± 3 percent (fig. 5(a)). At the rotor outlet, the difference between the integrated flows and the measured Venturi flows is as high as 14 percent (fig. 5(b)). The differences are somewhat greater at low flow, indicating the increasing effect of small errors in angle measurement (0.5°) as the outlet flow angles increase in value. Additional factors contributing to the difficulty in obtaining agreement at the outlet measuring station are discussed in reference 9.

Visual studies of the cavitation within the rotor blade row were made only in 80° F (300 K) water because of a temperature limitation of the plastic window. Still photographs were obtained at various rotor speeds and flow coefficients.

RESULTS AND DISCUSSION

Noncavitation and cavitation performance of the pump and rotor in deaerated water at temperatures to 250° F (394 K) were obtained. Cavitation formations in the rotor flow passages were observed and photographed in 80° F (300 K) water. The rotor blades sustained slight cavitation damage during the 162 hours of operation.

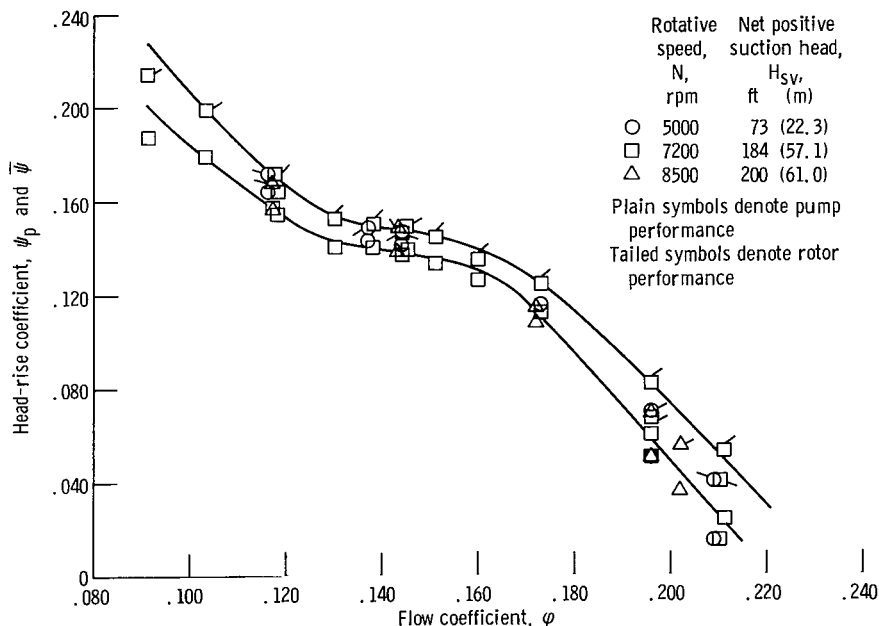


Figure 6. - Noncavitation performance of pump and rotor in 80° F (300 K) water at three rotative speeds.

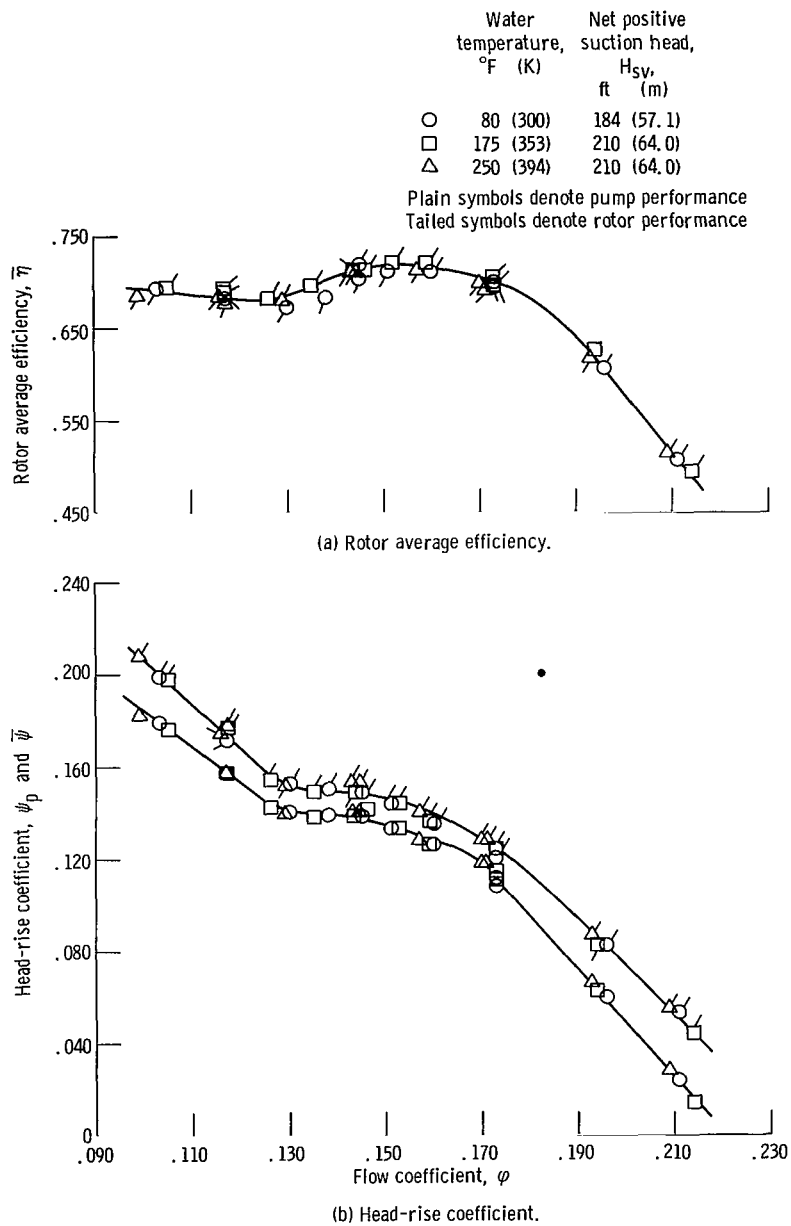


Figure 7. - Noncavitation performance of pump and rotor at three water temperatures and rotative speed of 7200 rpm.

Noncavitating Performance

Noncavitating performance of the pump and rotor at rotational speeds of 5000, 7200, and 8500 rpm and an inlet water temperature of 80° F (300 K) is shown in figure 6. Figure 7 shows similar performance curves for operation at 7200 rpm and inlet water temperatures of 80°, 175°, and 250° F (300, 353, and 394 K). All of these data were taken with sufficiently high inlet pressures that cavitation did not affect overall performance. The head-rise coefficient curves which are faired the same in figures 6 and 7 show that neither rotational speed nor water temperature affected the noncavitating overall performance. The head-rise coefficient curve shows a marked inflection near the rotor design flow coefficient of 0.147.

Rotor head-rise coefficient is higher than overall pump head-rise coefficient because of the losses in the pump inlet, the outlet vaneless diffuser, and volute collector. The degradation of pump head-rise coefficient will be utilized in the following discussion as a measure of the cavitation effect on pump performance. A peak calculated rotor efficiency of 0.71 is indicated at the design flow coefficient in figure 7. Efficiency varies within a relatively narrow band up to a flow coefficient of 0.18 and then drops rather sharply.

Cavitation Performance at 80° F (300 K)

Pump cavitation performance in 80° F (300 K) water and rotative speeds of 5000, 7200, and 8500 rpm for a nominal flow coefficient of 0.118 is shown in figure 8(a). Similar performance curves for flow coefficients of 0.144 (near design) and 0.173 are shown in figures 8(b) and (c), respectively. Head-rise coefficient ratio ($\psi_p/\psi_{p,max}$) is a normalized form of pump head-rise coefficient. For this rotor the maximum head-rise coefficient occurs just before dropoff. This maximum value is usually greater than the noncavitating head-rise coefficient which is obtained at a higher value of net positive suction head. The net positive suction head required to avoid the dropoff in performance increases with rotational speed and flow coefficient.

The region of performance dropoff has been replotted in figure 9 as a function of suction head coefficient ψ_{sv} , which equals gH_{sv}/U_t^2 . Suction head coefficient is a dimensionless form of net positive suction head and is defined in appendix B. Within the limits of data scatter, a single curve is generated for each flow coefficient over the range of rotative speeds investigated. The required suction head coefficient to achieve a given head coefficient ratio increases with increasing flow coefficient. The slope of the 0.144 flow coefficient performance curve is considerably less than that for either the higher or lower flow coefficients. This flow coefficient is near the design value at which inflection

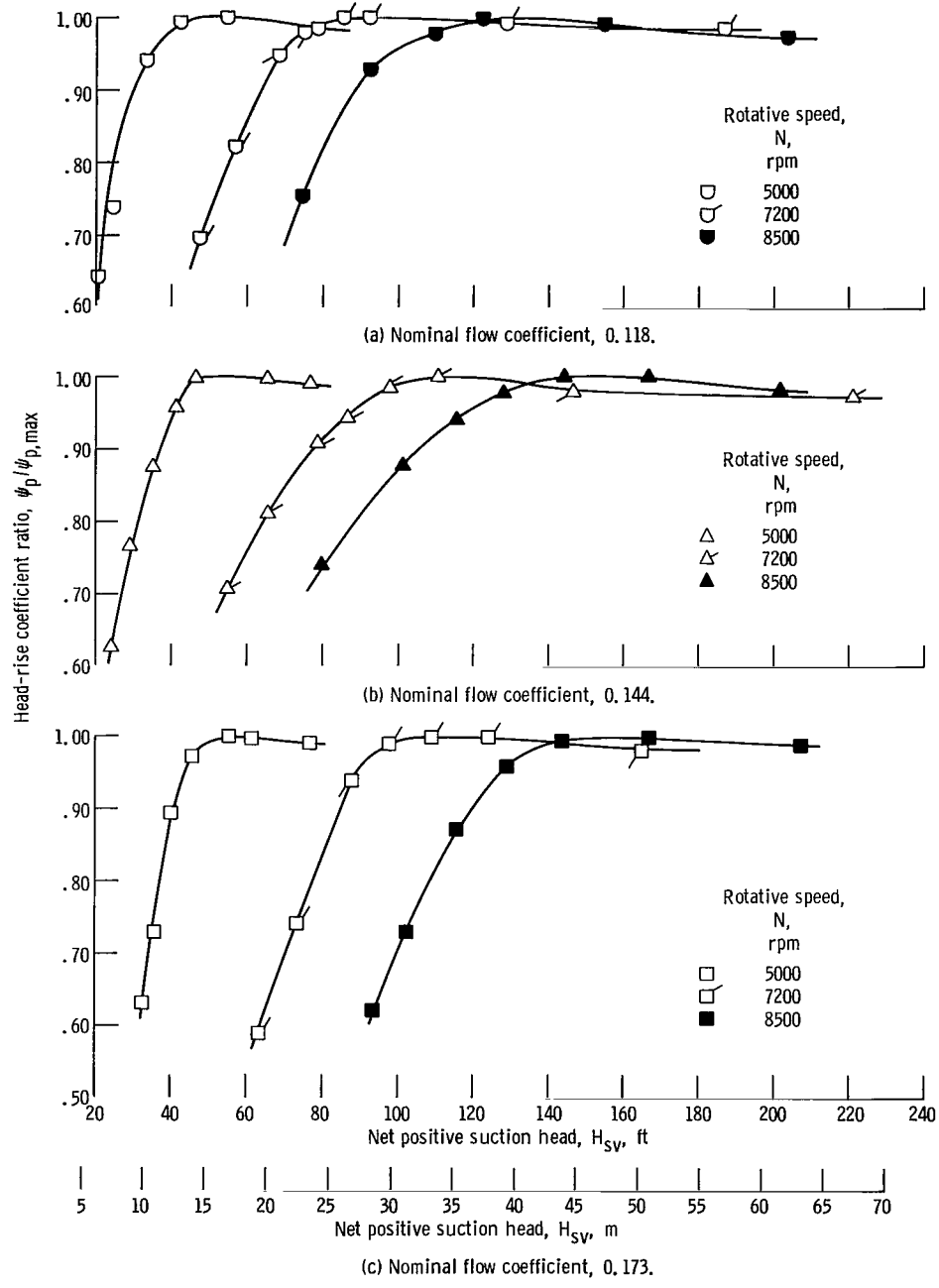


Figure 8. - Pump cavitation performance at water temperature of 80° F (300 K) and three nominal flow coefficients.

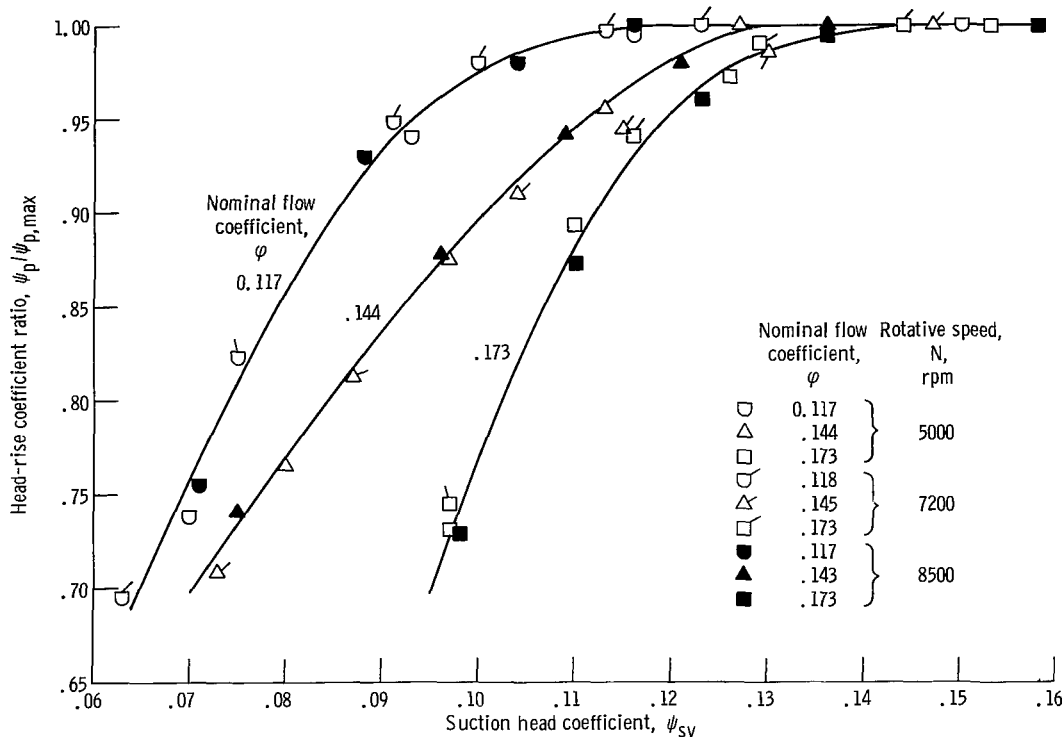


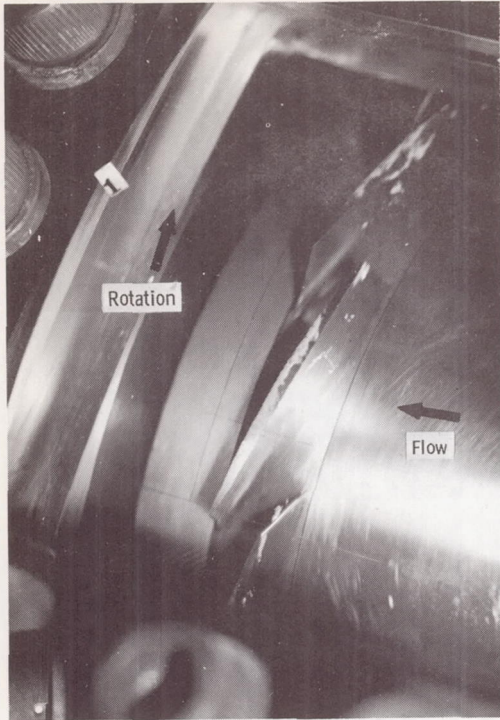
Figure 9. - Pump normalized cavitation performance in 80° F (300 K) water at three rotative speeds and three nominal flow coefficients.

was observed in the noncavitating performance curves of figures 6 and 7. Pump operation was stable even in deep cavitation or low values of head-rise coefficient ratio. Initial performance falloff occurs at a suction specific speed S_s between 5500 and 6000. At a head-rise coefficient ratio of 0.90, suction specific speed is between 6500 and 7000.

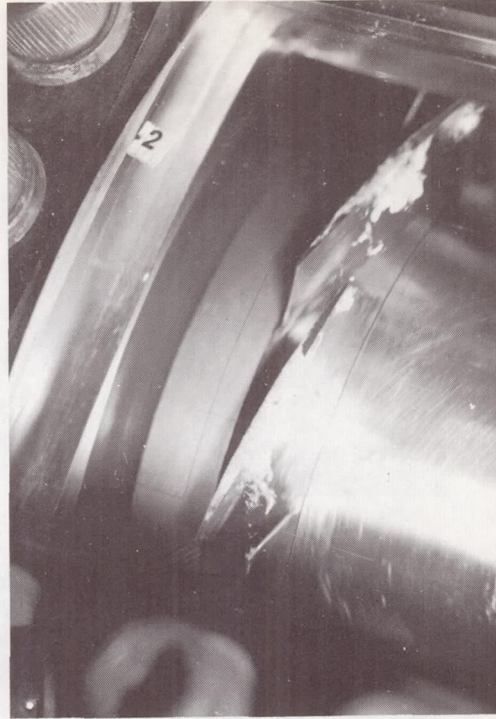
Photographs of Cavitation Formations in the Rotor

Photographs of cavitation in the rotor flow passages at selected performance test points are presented in figures 10 to 13. Water temperature was 80° F (300 K).

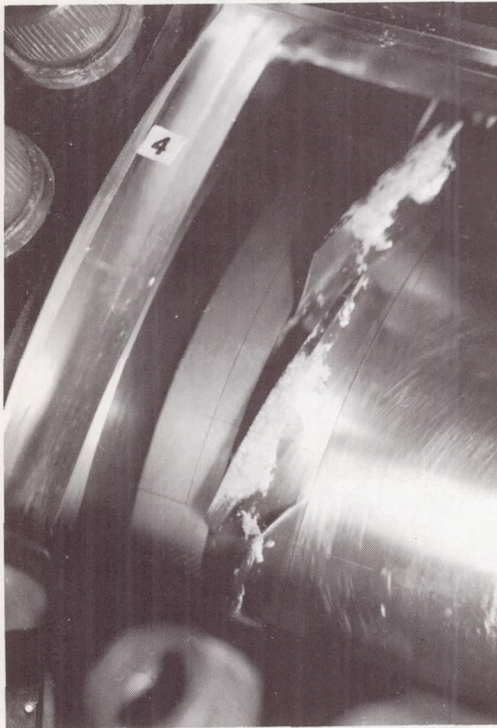
Cavitation formations in the rotor at a constant flow coefficient of 0.145 are presented in figure 10 at decreasing values of net positive suction head. Pump rotative speed is 7200 rpm. Pump performance is unaffected by cavitation at the test point represented in figure 10(a). Suction specific speed is approximately 4000. Head-rise coefficient ratio decreases to 0.91 in figure 10(c) and to 0.81 in figure 10(d). The photographs indicate that tip vortex cavitation increased in volume and extended rearward with decreasing net positive suction head (increasing suction specific speed). In addition, visual observation indicates that the cavitation cloud extends radially inward with decreasing net positive suction head. Initial head-rise dropoff occurred when tip vortex cavitation



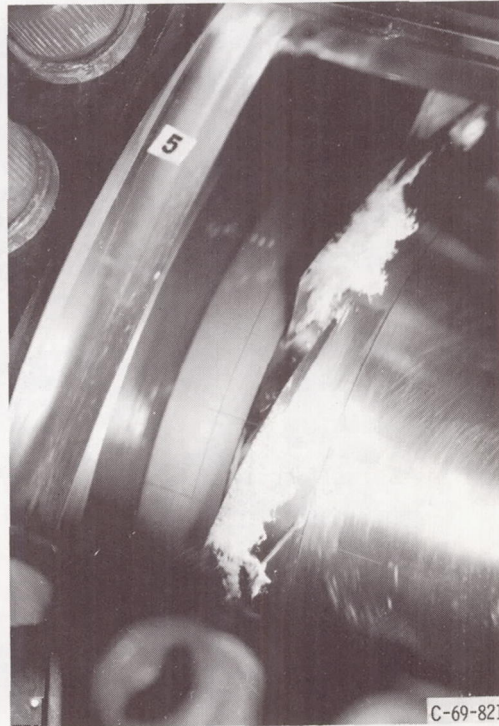
(a) $H_{SV} = 147$ feet (44.8 m); $\psi_p/\psi_{p, \max} = 1.0$.



(b) $H_{SV} = 98$ feet (29.8 m); $\psi_p/\psi_{p, \max} = 0.99$.



(c) $H_{SV} = 78$ feet (23.8 m); $\psi_p/\psi_{p, \max} = 0.91$.



(d) $H_{SV} = 65$ feet (19.8 m); $\psi_p/\psi_{p, \max} = 0.81$.

Figure 10. - Cavitation formations in 80° F (300 K) water at four net positive suction heads. Flow coefficient, 0.145; rotative speed, 7200 rpm. (Net positive suction head, H_{SV} ; head-rise coefficient ratio, $\psi_p/\psi_{p, \max}$.)

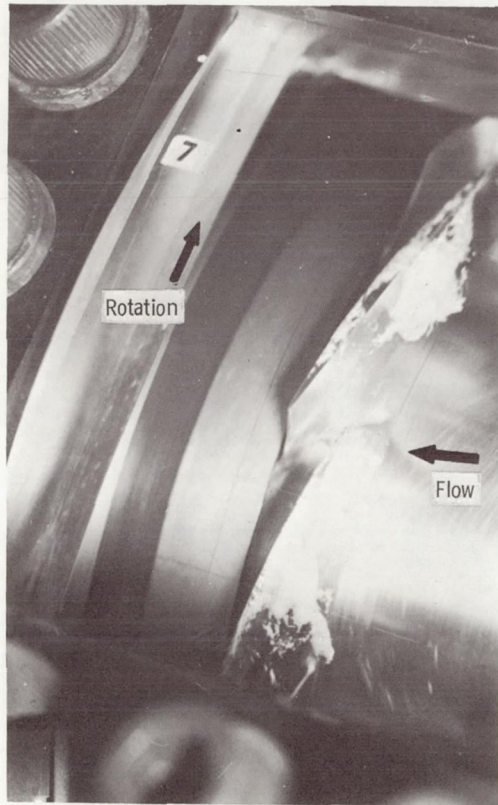
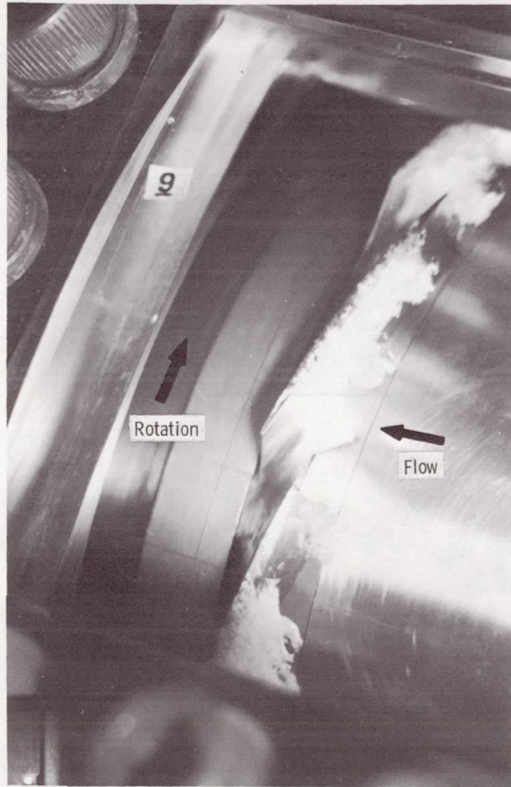
(a) $\varphi = 0.118$.(b) $\varphi = 0.145$.(c) $\varphi = 0.173$.

Figure 11. - Cavitation formations in 80° F (300 K) water at three flow coefficients. Suction specific speed, 6000; rotative speed, 7200 rpm; head-rise coefficient ratios range between 0.99 and 0.94. (Flow coefficient, φ .)



(a) $\varphi = 0.118$.



(b) $\varphi = 0.145$.



(c) $\varphi = 0.173$

Figure 12. - Cavitation formations in 80° F (300 K) water at three flow coefficients. Suction specific speed, 7400; rotative speed, 7200 rpm; head-rise coefficient ratios range between 0.83 and 0.76. (Flow coefficient, φ .)

covered about the outer third of the flow passage. Most of the cavitation shown in figure 10 appears to originate in the low pressure cores of the blade tip vortices. These vortices are generated by interaction between secondary blade tip clearance flow and the main stream throughflow. Tip vortex cavitation penetrates further across the flow passage as it moves downstream. Apparently there is little impingement of tip vortex cavitation on the pressure surfaces of the following blades.

There is very little suction surface cavitation in figure 10. A small amount of vapor forms near the blade tips and trails back from the leading edges. The tip leading edge cavitation apparently generated the slight suction surface damage discussed in the section on cavitation damage.

The two sets of three photographs in figures 11 and 12 each illustrate the effect of flow coefficient on the rotor cavitation formations at a rotative speed of 7200 rpm. The photographs in figure 11 show the cavitation formations for the three nominal flow coefficients at initial head-rise dropoff (suction specific speed of approximately 6000). The head-rise coefficient ratios range from 0.94 to 0.99. Figure 12 shows the cavitation formations at the same nominal flow coefficients at substantially lower head-rise coefficient ratios from 0.76 to 0.83. Flow coefficient range for each set is 0.118 to 0.173.

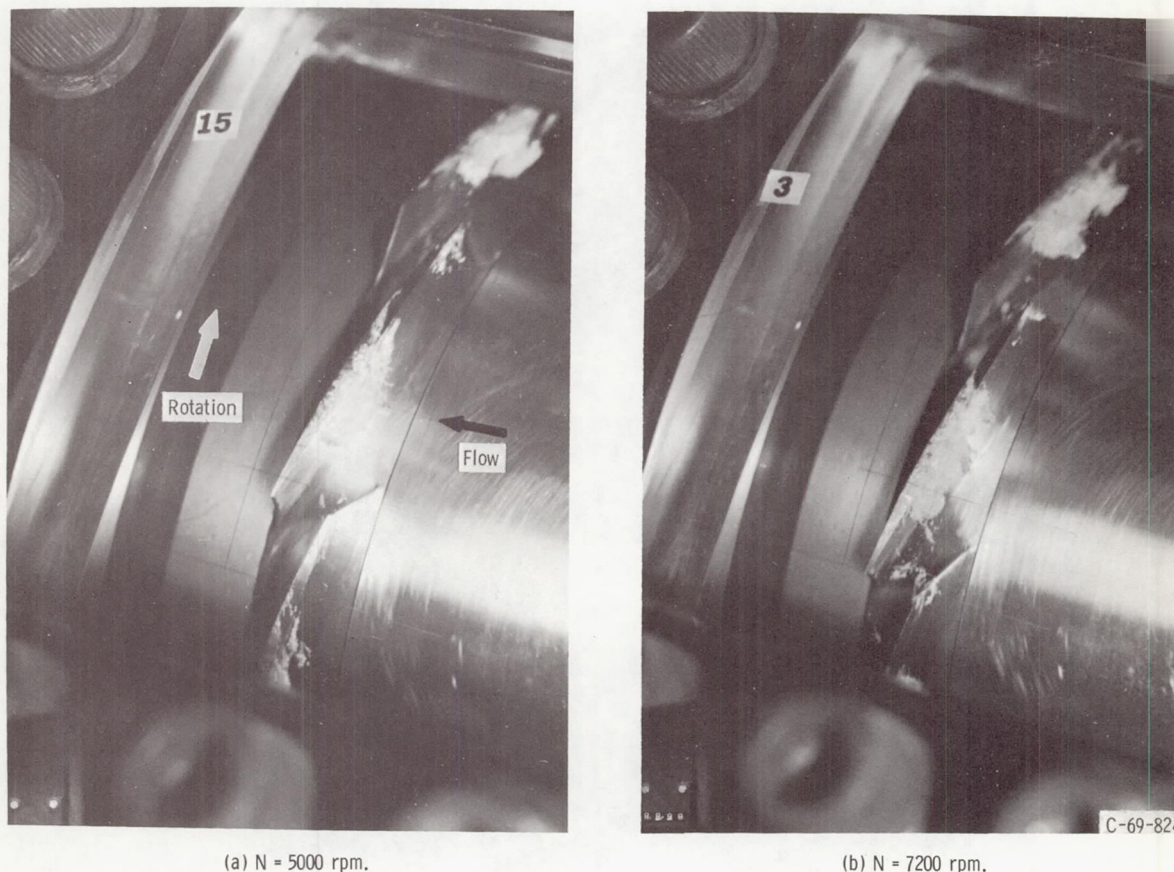


Figure 13. - Cavitation formations in 80° F (300 K) water at two rotative speeds. Flow coefficient, 0.145; nominal suction specific speed, 5980; head-rise coefficient ratio, 0.95. (Rotative speed, N.)

Each set of three photographs indicates the effect of flow coefficient on the tip vortex cavitation. At low flow coefficient tip vortex cavitation penetrates the flow passage to a marked degree. Increasing the flow causes the region of cavitation to occur closer to the blade.

The photographs of figure 13 show rotor cavitation formations at rotative speeds of 5000 and 7200 rpm. The rotor was operating at a flow coefficient of 0.145 (near design), and the inlet pressure level was set to provide a suction specific speed of approximately 5980 for both speeds. This corresponds to a ψ_{sv} of about 0.11. Head-rise coefficient ratio is approximately the same at the two conditions (0.95 to 0.96). As expected, the cavitation formations were of about the same extent at equivalent suction specific speeds since this parameter is useful in correlating head-rise falloff.

Cavitation Performance at Elevated Temperatures

Cavitation performance is presented in figures 14 to 16 at a rotative speed of 7200 rpm and at three temperatures, 80^o, 175^o, and 250^o F (300, 353, and 394 K). The reference fluid temperature is considered to be 80^o F (300 K) since there is no measurable cavitation performance improvement over that at a lower temperature (ref. 2).

Pump head-rise coefficient ratio is shown in figure 14 as a function of required net positive suction head at each of the three nominal flow coefficients previously discussed. In all cases the performance curve at 175^o F (353 K) is coincident with the 80^o F (300 K) performance curve. However, at 250^o F (394 K) the net positive suction head required to achieve a given head-rise coefficient ratio is less than that required at 80^o or 175^o F (300 or 353 K) water temperature. This reduction in required net positive suction head is attributed to the change of the thermodynamic properties of the fluid being pumped (ref. 2) and the effects on the phase change process involved when cavitation occurs.

The thermodynamic effects of cavitation were shown (fig. 14) to vary with nominal flow coefficients. The curves are cross plotted in figure 15 to obtain the required H_{sv} as a function of flow coefficient for head-rise coefficient ratios of 0.9, 0.8, and 0.7. The thermodynamic effect of cavitation observed at 250^o F (394 K) at a given head-rise coefficient ratio is the difference in the required net positive suction heads of figure 14 or 15. This difference is shown as the thermodynamic effect of cavitation in figure 16 for the range of nominal flow coefficients investigated and for head-rise coefficient ratios of 0.90, 0.80, and 0.70. The thermodynamic effect of cavitation is about 1.8 feet (0.55 m) at the low flow coefficient for the three levels of head-rise coefficient ratio. The thermodynamic effect increases with increasing flow coefficient or with decreasing head-rise coefficient ratio.

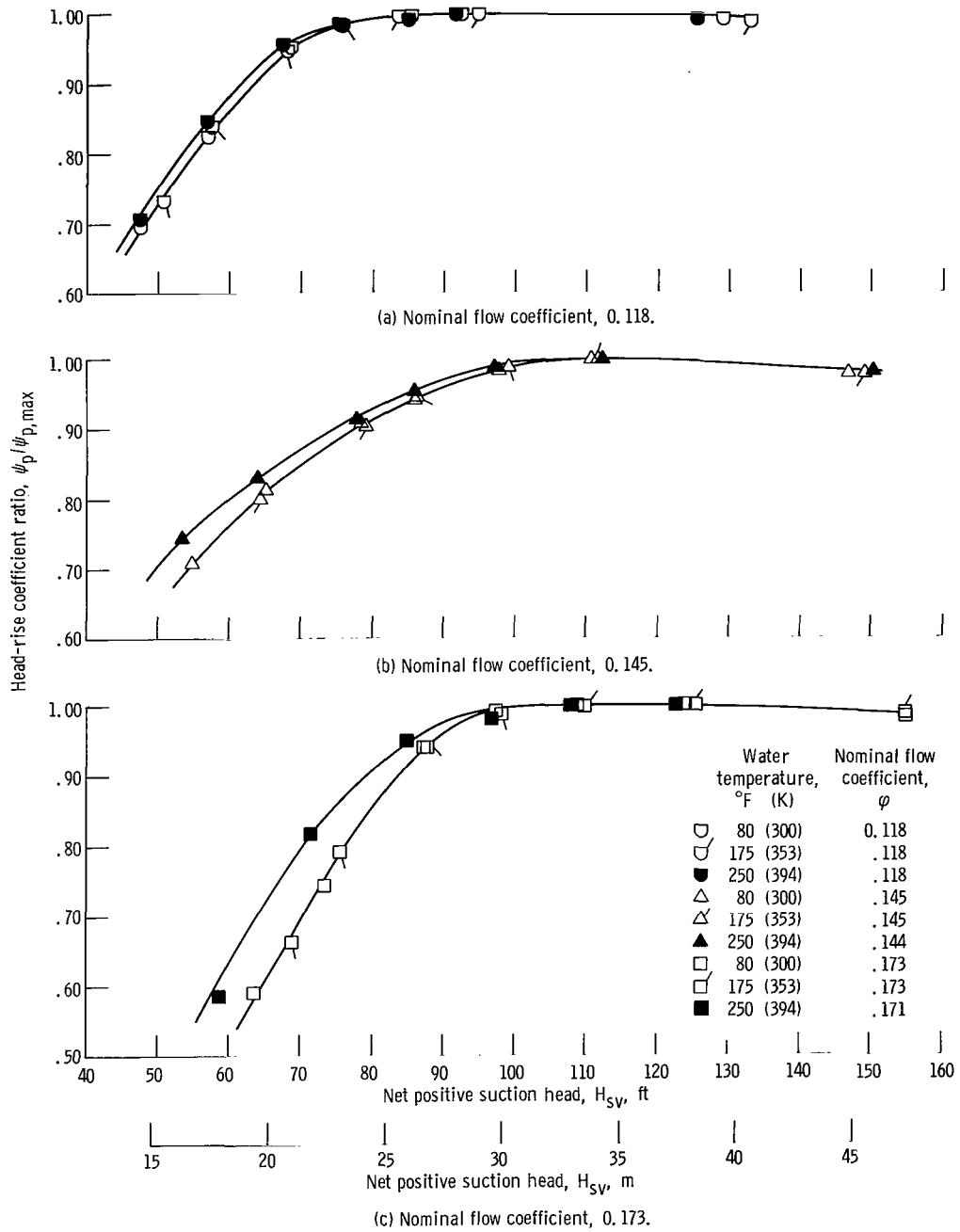


Figure 14. - Pump cavitation performance at three nominal flow coefficients, three temperatures, and rotational speed of 7200 rpm.

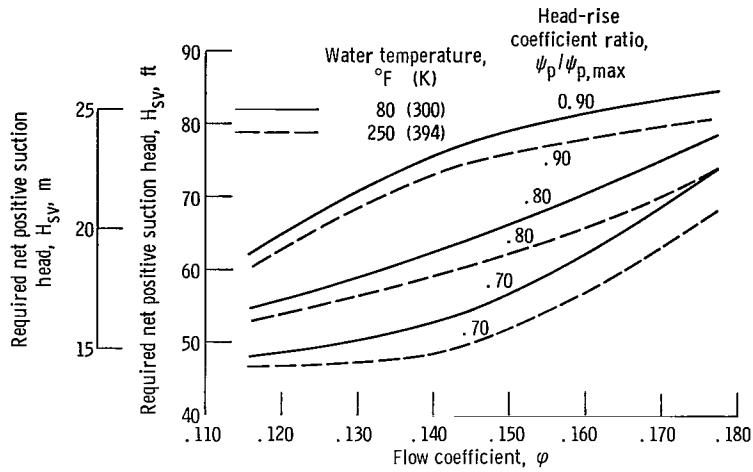


Figure 15. - Required net positive suction head in water at 80° and 250° F (300 and 394 K) for three head-rise coefficient ratios at rotative speed of 7200 rpm.

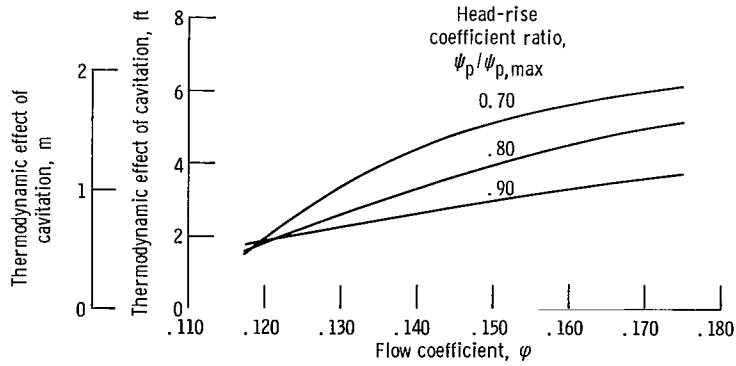
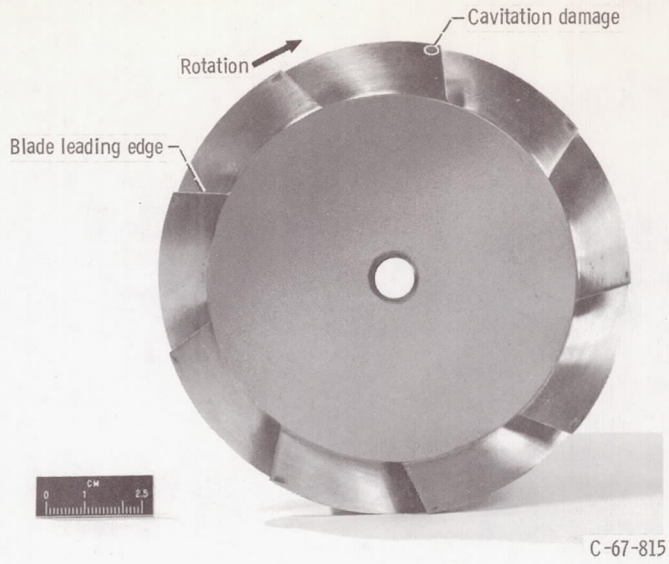
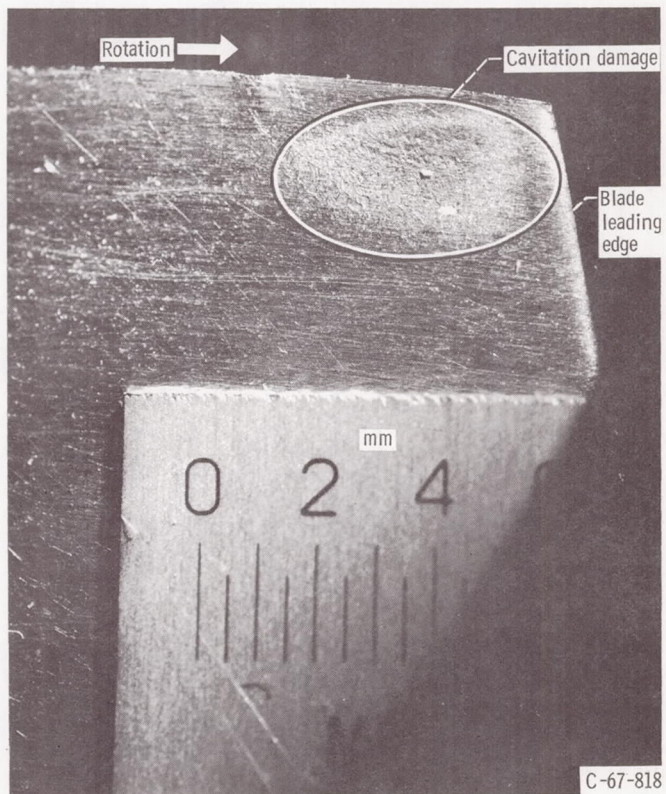


Figure 16. - Thermodynamic effect of cavitation at water temperature of 250° F (394 K) and rotative speed of 7200 rpm.



(a) Front view.



(b) Enlarged photograph.

Figure 17. - Post-test view of rotor showing suction surface cavitation damage.

The trend of increased thermodynamic effect of cavitation with flow coefficient is opposite to that reported in reference 10 for a flat plate helical inducer in liquid hydrogen. Observation of helical rotors indicates that dropoff in performance is usually experienced as a result of extensive blade surface cavitation. The axial flow rotor used in this investigation appears to experience performance dropoff because of the relatively large tip vortex cavitation without appreciable blade surface cavitation. In addition to the difference in fluid properties of the two tests, other differences include rotor geometry and the design level of suction specific speed.

Rotor Blade Cavitation Damage

The rotor sustained only minor suction surface cavitation damage near the blade tip leading edges. This damage is shown in figure 17(a), which is a photograph of a front view of the rotor. This rotor logged about 162 hours of operating time during this investigation, of which 71 hours were in cavitation. Figure 17(a) shows that the damage is relatively minor and similar in location and size on each blade. A closeup photograph of the damaged area is shown in figure 17(b). In this photograph the damage appears as a lighter surface than that of the rest of the blade. This damage is similar in size, location, and severity to that sustained in the tests of a similar rotor in liquid sodium described in reference 6. This damage is attributed to tip leading edge cavitation.

SUMMARY OF RESULTS

A 5-inch (12.7-cm) axial flow rotor was tested in deaerated water at temperatures of 80^o, 175^o, and 250^o F (300, 353, and 394 K). Noncavitation and cavitation performance of the rotor and pump was obtained at rotative speeds of 5000, 7200, and 8500 rpm in 80^o F (300 K) water. Photographs of the cavitation formations in the rotor were taken in 80^o F (300 K) water. Performance at the two higher temperatures was obtained at 7200 rpm. The following experimental results were obtained:

1. Pump cavitation performance is independent of fluid temperature to 175^o F (353 K). A reduction in the required net positive suction head of 2.0 to 6.0 feet (0.6 to 1.8 m) was measured in 250^o F (394 K) water under that in room temperature water at similar operating conditions. This improvement in cavitation performance is attributed to the thermodynamic effects of cavitation, and is increased with increasing flow coefficient and decreasing head-rise coefficient ratio. At a head coefficient ratio of 0.90 and at the design flow coefficient of 0.147, the measured reduction in required net positive suction head is 2.9 feet (0.9 m) between 80^o and 250^o F (300 and 394 K).

2. Noncavitation performance is unaffected by temperature in the range of 80^o to 250^o F (300 to 394 K). An inflection of the head flow characteristic curve occurs near design flow coefficient.

3. Visual observations and photographs indicate that cavitation appears at fairly low suction specific speeds (≈ 4000) long before performance is affected. Initial head-rise dropoff occurs at suction specific speeds of 5500 to 6000 when tip vortex cavitation over the middle third of the blade chord covers the outer third of the flow passage. The tip vortex cavitation occurs closer to the blade with increasing flow coefficient. The cavitation formations at different rotative speeds are markedly similar at equal suction specific speeds. Very little suction surface cavitation occurs within the rotor.

4. The rotor blades sustained minor suction surface cavitation damage near the tip leading edges. This damage is attributed to small tip leading edge cavitation. The damage on each blade was very similar in severity, location, and size. Rotor damage was similar to that sustained by a similar rotor in previous liquid sodium tests.

Lewis Research Center,

National Aeronautics and Space Administration,

Cleveland, Ohio, February 28, 1969,

128-31-32-12-22.

APPENDIX A

SYMBOLS

c	blade chord, ft (m)	ν	kinematic viscosity, ft ² /sec (m ² /sec)
D	blade diffusion factor	σ	rotor solidity, c/s
g	acceleration due to gravity, 32.17 ft/sec ² (9.86 m/sec ²)	φ	flow coefficient
H	total head, ft (m)	ψ	head-rise coefficient
ΔH	head rise, ft (m)	ψ_{sv}	suction head coefficient
H_{av}	net positive suction head, ft (m)	Subscripts:	
h	static head, ft (m)	e	error
h_v	vapor head, ft (m)	h	hub
N	rotative speed, rpm	i	ideal
Q	flow rate, gal/min (m ³ /sec)	max	maximum
Re_p	blade chord Reynolds number	p	pump
r	radius, in. (m)	t	tip
S_s	suction specific speed, $N\sqrt{Q}/(H_{sv})^{3/4}$	v	as measured by Venturi flowmeter
s	blade tangential spacing, ft (m)	z	axial direction
U	rotor tangential velocity, ft/sec (m/sec)	θ	tangential direction
V	absolute fluid velocity, ft/sec (m/sec)	0	measuring station at pump inlet
β	flow angle with respect to rotor axis, deg	1	measuring station at rotor inlet
η	efficiency, percent	2	measuring station at rotor outlet
		3	measuring station at pump outlet
		Superscripts:	
		—	average or overall value
		'	relative to rotor

APPENDIX B

CALCULATIONS

Rotor Blade Element (at Each Radial Station)

Head rise:

$$\Delta H = H_2 - H_1$$

Ideal head rise:

$$\Delta H_i = UV_{\theta,2}/g \quad (\text{assuming } V_{\theta,1} = 0)$$

Efficiency:

$$\eta = \frac{\Delta H}{\Delta H_i}$$

Head-rise coefficient:

$$\psi = \frac{g \Delta H}{U_t^2}$$

Ideal head-rise coefficient:

$$\psi_i = \frac{g \Delta H_i}{U_t^2}$$

Velocity:

$$V = \sqrt{2g(H - h)}$$

Axial velocity:

$$V_z = V \cos \beta$$

Overall Rotor Performance

Average axial velocity:

$$\bar{V}_z = \frac{0.10214 Q_v}{r_t^2 - r_h^2}$$

Flow coefficient:

$$\varphi = \frac{\bar{V}_z}{U_t}$$

Integrated volume flow rate:

$$Q = 19.58 \int_{r_h}^{r_t} V_z r \, dr$$

Percentage error between integrated and Venturi volume flows:

$$Q_e = 1 - \frac{Q}{Q_v}$$

Mass-averaged rotor total head:

$$\bar{H} = \frac{\int_{r_h}^{r_t} r V_z H \, dr}{\int_{r_h}^{r_t} V_z \, dr}$$

Mass-averaged rotor head rise:

$$\Delta \bar{H} = \bar{H}_2 - \bar{H}_1$$

Mass-averaged rotor head-rise coefficient:

$$\bar{\psi} = \frac{g}{U_t^2} (\bar{H}_2 - \bar{H}_1)$$

Mass-averaged rotor efficiency:

$$\bar{\eta} = \frac{\int_{r_h}^{r_t} r V_z \eta \, dr}{\int_{r_h}^{r_t} r V_z \, dr}$$

Overall Pump Performance

Pump inlet total head:

$$H_0 = h_0 + \frac{\bar{V}_0^2}{2g}$$

Pump outlet total head:

$$H_3 = h_3 + \frac{\bar{V}_3^2}{2g}$$

Pump total head rise:

$$\Delta H_p = H_3 - H_0$$

Pump head-rise coefficient:

$$\psi_p = \frac{g \Delta H_p}{U_t^2}$$

Net positive suction head:

$$H_{sv} = H_0 - h_v$$

Suction head coefficient:

$$\psi_{sv} = g \frac{H_{sv}}{U_t^2}$$

Blade chord Reynolds number:

$$Re_b = \frac{V_{t,1} c}{\nu_1}$$

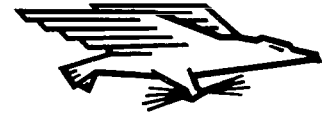
Blade diffusion factor:

$$D = 1 - \frac{V'_2}{V'_1} + \frac{V'_{\theta,2} - V'_{\theta,1}}{2\sigma V'_1}$$

REFERENCES

1. Kerr, B. M.; Day, M. S.; Howick, G. J.; Lesher, R. L.; and Timms, H. L.: Technology Utilization. Selected Technology for the Petroleum Industry. NASA SP-5053, 1966, pp. 155-166.
2. Stepanoff, A. J.: Cavitation Properties of Liquid. J. Eng. Power, vol. 86, no. 2, Apr. 1964, pp. 195-200.
3. Gelder, Thomas F.; Ruggeri, Robert S.; and Moore, Royce D.: Cavitation Similarity Considerations Based on Measured Pressure and Temperature Depressions in Cavitated Regions of Freon 114. NASA TN D-3509, 1966.
4. Jakobsen, J. K.: On the Mechanism of Head Breakdown in Cavitating Inducers. J. Basic Eng., vol. 86, no. 2, June 1964, pp. 291-305.
5. Spraker, W. A.: The Effects of Fluid Properties on Cavitation in Centrifugal Pumps. Paper 64-WA-FE-14, ASME, Dec. 1964.
6. Reemsnyder, Dean C.; Cunnan, Walter S.; and Weigel, Carl: Performance and Cavitation Damage of an Axial-Flow Pump in 1500⁰ F (1089 K) Liquid Sodium. NASA TN D-5138, 1969.
7. Crouse, James E.; Montgomery, John C.; and Soltis, Richard F.: Investigation of the Performance of an Axial-Flow-Pump Stage Designed by the Blade-Element Theory - Design and Overall Performance. NASA TN D-591, 1961.
8. Johnsen, Irving A.; and Bullock, Robert O., eds.: Aerodynamic Design of Axial-Flow Compressors. NASA SP-36, 1965.
9. Soltis, Richard F.; Anderson, Douglas A.; and Sandercock, Donald M.: Investigation of the Performance of a 78⁰ Flat-Plate Helical Inducer. NASA TN D-1170, 1962.
10. Meng, Phillip R.: Change in Inducer Net Positive Suction Head Requirement with Flow Coefficient in Low Temperature Hydrogen (27.9⁰ R to 36.6⁰ R). NASA TN D-4423, 1968.

FIRST CLASS MAIL



POSTAGE AND FEES PAID
NATIONAL AERONAUTICS AND
SPACE ADMINISTRATION

NOV 17 1958
MAIL ROOM
NATIONAL AERONAUTICS AND SPACE ADMINISTRATION
WASHINGTON, D. C. 20546

NOV 17 1958
MAIL ROOM
NATIONAL AERONAUTICS AND SPACE ADMINISTRATION
WASHINGTON, D. C. 20546

POSTMASTER: If Undeliverable (Section 158
Postal Manual) Do Not Return

"The aeronautical and space activities of the United States shall be conducted so as to contribute . . . to the expansion of human knowledge of phenomena in the atmosphere and space. The Administration shall provide for the widest practicable and appropriate dissemination of information concerning its activities and the results thereof."

— NATIONAL AERONAUTICS AND SPACE ACT OF 1958

NASA SCIENTIFIC AND TECHNICAL PUBLICATIONS

TECHNICAL REPORTS: Scientific and technical information considered important, complete, and a lasting contribution to existing knowledge.

TECHNICAL NOTES: Information less broad in scope but nevertheless of importance as a contribution to existing knowledge.

TECHNICAL MEMORANDUMS: Information receiving limited distribution because of preliminary data, security classification, or other reasons.

CONTRACTOR REPORTS: Scientific and technical information generated under a NASA contract or grant and considered an important contribution to existing knowledge.

TECHNICAL TRANSLATIONS: Information published in a foreign language considered to merit NASA distribution in English.

SPECIAL PUBLICATIONS: Information derived from or of value to NASA activities. Publications include conference proceedings, monographs, data compilations, handbooks, sourcebooks, and special bibliographies.

TECHNOLOGY UTILIZATION PUBLICATIONS: Information on technology used by NASA that may be of particular interest in commercial and other non-aerospace applications. Publications include Tech Briefs, Technology Utilization Reports and Notes, and Technology Surveys.

Details on the availability of these publications may be obtained from:

**SCIENTIFIC AND TECHNICAL INFORMATION DIVISION
NATIONAL AERONAUTICS AND SPACE ADMINISTRATION
Washington, D.C. 20546**